Islamic Azad University

Journal of

Optoelectronical Nanostructures

Spring 2018 / Vol. 3, No. 2

Analysis of InGaAsP-InP Double Microring Resonator using Signal Flow Graph Method

Mahdi Bahadoran[*,1]

[1] Department of Physics, Shiraz University of Technology 31371555, Shiraz, Fars, Iran.

(Received 20 Mar. 2018; Revised 14 Apr 2018; Accepted 23 May 2018; Published 15 Jun. 2018)

Abstract: The buried hetero-structure (BH) InGaAsP-InP waveguide is used for a system of double microring resonators (DMR). The light transmission and location of resonant peaks are determined for six different sets of ring radii with different order mode numbers. The effect of changing middle coupling coefficient on the box like response is studied. It is found that the surge of coupling coefficient to the lower values makes the through port resonance peaks sharper and for a larger amount of middle coupling values, the transmission decreases according to the order mode numbers. The DMR design with a small middle coupling and close values for rings perimeters can generate practical pass bandwidth of the resonant transmission peak. Moreover, any modification in resonant mode numbers and middle coupling coefficient can change the width and height of the box like response. A DMR simulated results with the free spectral range (FSR) of 10.2 nm is validated by comparing with the experimental data. Achieved results are practical in the filtering process of optical communication.

Keywords: Double Ring Resonator ; Microring Resonator, Signal Flow Graph; Optical Filter.

1. INTRODUCTION

Microring resonators have been receiving considerable attention due to extensive use in optoelectronics [1], photonics sensors and biosensors [2, 3] and optical communication[4, 5]. Dense Wavelength Division Multiplexing (DWDM) systems required an extended free spectral range (FSR) or channel spacing in order to accommodate large channel counts. Optical channel filters have this ability to separate two adjacent channels which is practical in the DWDM systems. Two methods have been suggested to increase the FSR in the micro resonating systems. The first approach is to use single microring

* Corresponding author. E-mail: **bahadoran@sutech.ac.ir**

resonator with the minimum ring radius[6]. Since the FSR is inversely proportional to the radius of a ring[7], the maximum value for the FSR can be achieved by selecting the minimum value for the ring radius. However, this technique has a drawback in that it cannot expand the FSR very well. In practice, using small size of microring resonator as an optical tunable filter makes an essential problem for increasing channel spacing since the bending loss increased drastically by reducing the ring radius[8]. Employing the system, including multiple stages of microring resonators is another alternative to achieve a wide channel spacing[1]. This is a feasible approach, which contributes to embed large channel count in DWDM system and can increase the capacity of the optical system. The sharpness of output signals from a resonating system depends on the waveguide scattering loss. Since the waveguide loss is proportional to the refractive index of the core and cladding of the waveguide, the InGaAsP-InP material can be selected as a low-loss waveguide. In this paper, the characteristics of light filtering through a double microring resonator (DMR) are studied. For six different ring's radii with different order mode numbers, the light transmission and the location of resonant peaks are determined based on the value of the middle coupling coefficient. The simulated results are validated by comparing a sample of simulated results with experimental data.

2. OPTICAL TRANSFER FUNCTION

Several analytic methods have been developed in signal processing to calculate the optical transfer functions in the Z-domain[9]. These methods comprise of the scattering matrix method[10, 11][12, 13], the signal flow graph (*SFG*) method [14], and the transfer-matrix-chain-matrix algebraic method [15], which all used for the linear and time-invariant optical circuits. Amongst these methods the *SFG* method benefits from several advantages like graphic illustration of the signal flow via the system. Moreover, it provides a simple and methodical approach of manipulating the parameters of the system, beside the identification of the physical behavior and geometric properties of a system[16]. The channel spacing of the cascaded resonating system can be measured using the *SFG* method. The *FSR* denotes the frequency channel spacing, $FSR = \lambda^2 / n_{eff} L$, where λ, n_{eff} ,and L show the center wavelength, effective refractive index and the optical path of ring resonator, respectively. For a *DMR* system with two different rings, the extended *FSR* can be calculated by $FSR_{tot} = N_1.FSR_1 = N_2.FSR_2$ where FSR_1 and FSR_2 are free spectral range of ring 1 and ring 2 in the *DMR*. The parameters N_1 and N_2 are integer numbers known as resonant mode numbers. To avoid a mismatch of output resonances from cascaded resonator, the resonance condition, $n_{eff} L = N\lambda$, should be fulfilled. The layout of the double microring resonator (*DMR*) is illustrated in

Figure 1. Based on the *SFG* method, the optical transfer function of *DMR* at the through port is given by *[17]*

$$H_{thr}=\frac{E_{thr}}{E_{in}}=\frac{\begin{array}{l}\sqrt{(1-\gamma_1)(1-k_1)}-(1-\gamma_1)\times\\ \sqrt{(1-\gamma_2)(1-k_2)}e^{-(\alpha+\frac{i2\pi n_{eff}}{\lambda})(N_1L_1)}-e^{-(\alpha+\frac{i2\pi n_{eff}}{\lambda})(N_2L_2)}\times\\ \sqrt{(1-\gamma_1)(1-k_1)(1-\gamma_2)(1-k_2)(1-\gamma_3)(1-k_3)}+\\ (1-\gamma_1)(1-\gamma_2)\sqrt{(1-\gamma_3)(1-k_3)}e^{-(\alpha+\frac{i2\pi n_{eff}}{\lambda})(N_1L_1+N_2L_2)}\end{array}}{\begin{array}{l}1-\sqrt{(1-\gamma_1)(1-k_1)(1-\gamma_2)(1-k_2)}\;e^{-(\alpha+\frac{i2\pi n_{eff}}{\lambda})(N_1L_1)}+\\ -\sqrt{(1-\gamma_2)(1-k_2)(1-\gamma_3)(1-k_3)}\;e^{-(\alpha+\frac{i2\pi n_{eff}}{\lambda})(N_2L_2)}+\\ (1-\gamma_2)\sqrt{(1-\gamma_1)(1-k_1)(1-\gamma_3)(1-k_3)}\,e^{-(\alpha+\frac{i2\pi n_{eff}}{\lambda})(N_1L_1+N_2L_2)}\end{array}} \quad (1)$$

and the drop port optical transfer function is *[17]*

$$H_{drp}=\frac{E_{drp}}{E_{in}}=\frac{-i\sqrt{(1-\gamma_1)(1-\gamma_2)(1-\gamma_3)k_1k_2k_3}\,e^{-(\alpha+\frac{i2\pi n_{eff}}{\lambda})(N_1L_1+N_2L_2)}}{\begin{array}{l}1-\sqrt{(1-\gamma_1)(1-k_1)(1-\gamma_2)(1-k_2)}\;e^{-(\alpha+\frac{i2\pi n_{eff}}{\lambda})(N_1L_1)}+\\ -\sqrt{(1-\gamma_2)(1-k_2)(1-\gamma_3)(1-k_3)}\;e^{-(\alpha+\frac{i2\pi n_{eff}}{\lambda})(N_2L_2)}+\\ (1-\gamma_2)\sqrt{(1-\gamma_1)(1-k_1)(1-\gamma_3)(1-k_3)}\;e^{-(\alpha+\frac{i2\pi n_{eff}}{\lambda})(N_1L_1+N_2L_2)}\end{array}} \quad (2)$$

here k_n (*n=1,2,3*) shows the power coupling coefficient, γ_i (*i=1,2,3*) denotes the loss in coupling region, α , L , λ ,n_{eff}, N_1 and N_2 are the waveguide loss, the perimeter of each microring, the center wavelength of the channel, the effective refractive index , and the resonant mode numbers for rings 1 and 2, respectively. The intensity of the drop and the through ports of the *DMR* can be calculated by $I_{drp}=H_{drp}.H_{drp}^{*}$ and $I_{thr}=H_{thr}.H_{thr}^{*}$, respectively.

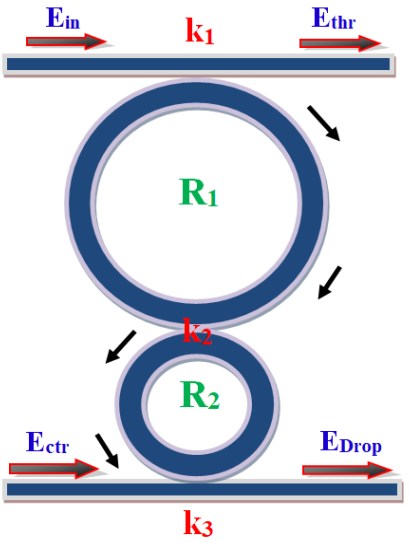

Fig. 1. Waveguide configuration of double stage microring resonator.

3. SIMULATED RESULT

The responses of the *DMR* system are simulated for various sets of middle coupling coefficients. The results are simulated for buried hetero-structure (*BH*) InGaAsP/InP micro resonator. The core of waveguide is the InGaAsP material with refractive index of 3.4, which is completely buried by InP material with refractive index of 3.17[18]. The waveguide scattering loss is proportional to the refractive indices of the core and cladding : $\alpha \sim (n_{core}^2 - n_{cladding}^2)$ [18], which lead to the low loss waveguide. The waveguide effective index of *neff =3.674* is used for simulation part. Results are simulated for *DMR* system, which is included ring's radii of 150.8 μm and 160.8 μm, the symmetric power coupling of *k1=k3=0.06*(6%), the field loss coefficient of 0.6 cm^{-1}. This *DMR* set up adjusted to achieve the *FSR* as large as 10.2 *nm*. The lateral couplers are fixed to be 3dB (*k1=k3=0.5*) and the values for middle coupler are selected to be 0.001, 0.5 and 0.9. Simulated results show that any change in middle coupling coefficient causes a variation in the number of resonant peaks. The box like response from the through port of the *DMR* is dealing with change of middle coupling coefficient as shown in the Figure 2 and 3. Increasing the value of middle coupler, *k2*, will change the main resonant peaks into dual resonances, which can shrink the *FSR*. The through port's extinction ratio(*ER*) for middle coupling of *k2=0.01* is about 0.89, which is dependent on coupling coefficient. The *ER* is correlated with the ring's radii ratio for a *DMR* design with the symmetric coupling coefficients (*k1=k2=k3=0.5*) as an increase in the mode

numbers contributes to increase the *ER*. In this case, the higher *ER* can be achieved by a design with the larger set of ring's radii. Increasing the middle coupling values and ring radii cause a fluctuation of *ER* in the range of 0.1 to *0.89* and will change the location of main resonant peaks as simulated in Figure 2 and 3.

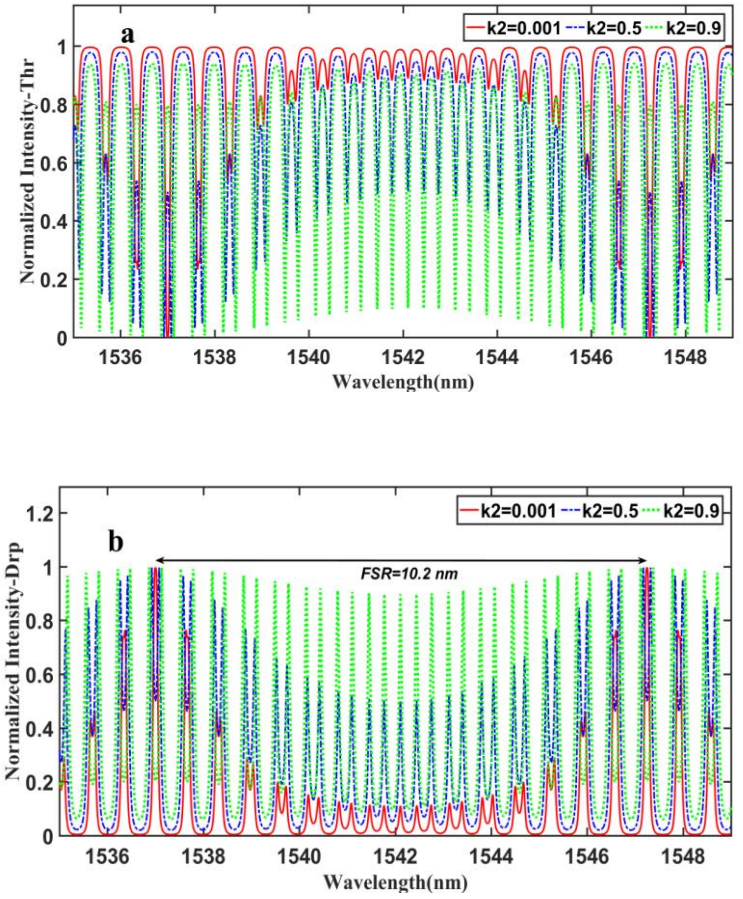

Fig. 2. The effect of changing the middle coupling coefficient of the DMR system on the *a)* normalized intensity at the through port. *b)* normalized intensity at the drop port.

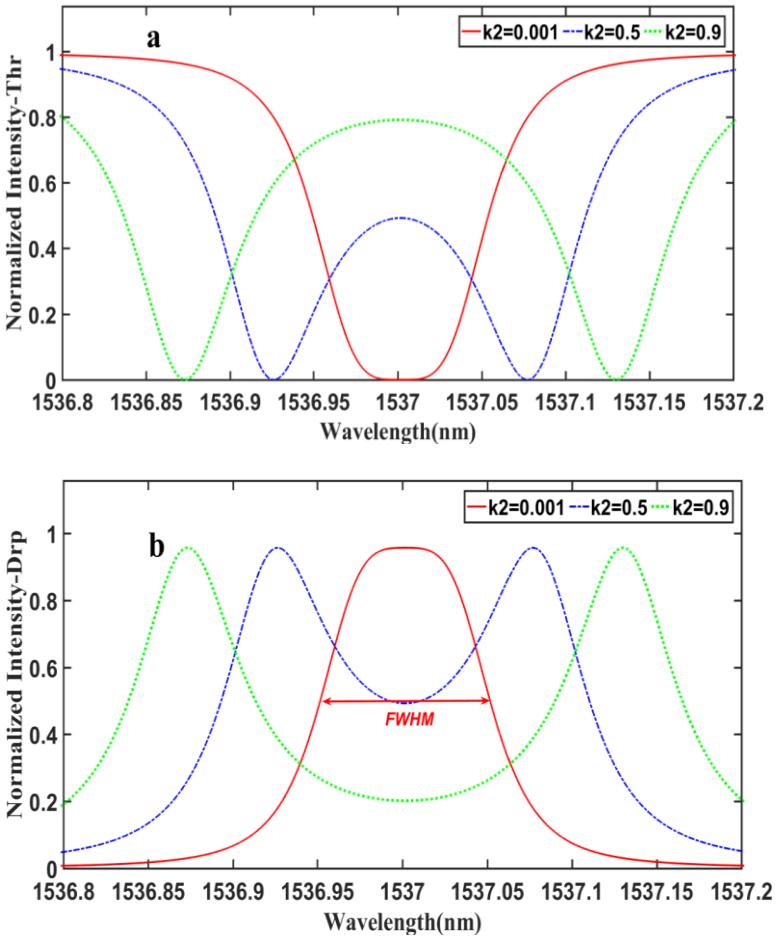

Fig. 3. The effect of changing the middle coupling coefficient of DMR system (*k1= k3=0.5*) on the resonance peaks at the a) through port b) drop port.

The effect of modifying middle coupling coefficient on the transmission of the drop port of the *DMR* system for different ring's radii, 3dB lateral coupling coefficients and various order mode numbers is shown in Figure 4. Amongst different layouts of the *DMR*, the highest flatness in resonant peaks were measured by the *DMR* system with identical ring's circumferences (Figure 3-a). The band rejection is the ability of a filter in differentiating the favorable and unfavorable signals on a specific wavelength/frequency band. The out of band rejection is the applied attenuation to the signals emerged outside the wavelength/frequency band around λo, which is calculated from

$OBRR = 10\log_{10}(I_{drop}^{\max} / I_{drop}^{\min})$. Here $I_{drop}^{\max}$ and $I_{drop}^{\min}$ are maximum and minimum intensities at the drop port.

The 3dB bandwidth for symmetric configuration was 1.59μm, and the out of band rejection ratio (*OBRR*) is measured to be 0.97 for *k=0.001.* It means that, the highest flatness for the drop port resonance peaks belong to the lower value of middle coupling (red line). Moreover, increase of k_2 is responsible for the reduction of resonance peaks as well as the quell of the interstitial resonances. The emergence of short lived and weak quench signals between main resonance peaks in the drop port is another consequence of increasing the middle coupling. The suppression of interstitial resonances for the drop port of the *DMR* is illustrated in Figure 3. The higher *OBRR* correlated with the suppression of inter-band cross talk. The more suppression in interstitial resonances can improve the band pass width, which can be achieved by the *DMR* layouts with smaller middle coupling coefficient.

In the last part, the light transmission and location of resonant peaks were specified from the drop port of *DMR* for six different sets of ring's radii with different order mode numbers as shown in Figure 4. Any variation of the mode-numbers brings about a modification in the intensity and the number of resonant peaks and contributes to a wavelength shift in resonant peaks. The change in resonant modes and middle coupling coefficient can change the width and height of the box like response. Suppression of interstitial resonance at the drop port of the *DMR* system for *k2=0.001*(red lines) are as follows: *0.89* for *(N1=1; N2=1)*, *0.87* for *(N1=2; N2=5)*, *0.36* for *(N1=5; N2=11)*, *0.24* for *(N1=15; N2=16)*, *0.78* for *(N1=8; N2=33)*, and *0.44* for *(N1=33; N2=91)*. In a DMR system with different ring radii, the interstitial resonances will not be quelled for large values of middle coupling coefficients (green dotted lines). Generally, the pass bandwidth of the resonant transmission peak is dominated by the *DMR* layout with a small value for middle coupler and close values for resonant mode numbers.

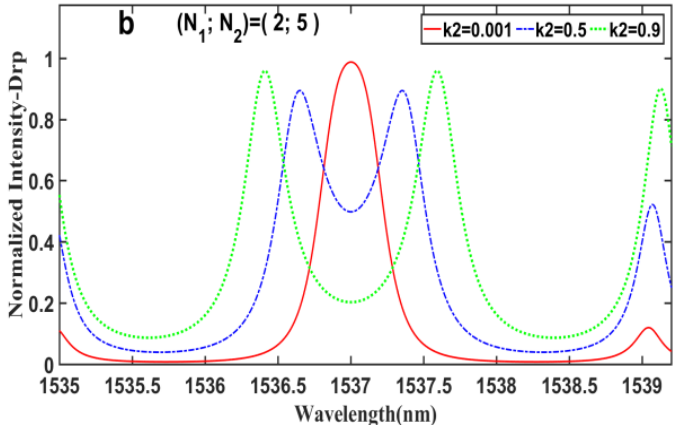
b
(N1; N2)=(2; 5)
k2=0.001
k2=0.5
k2=0.9
Normalized Intensity-Drp
Wavelength(nm)

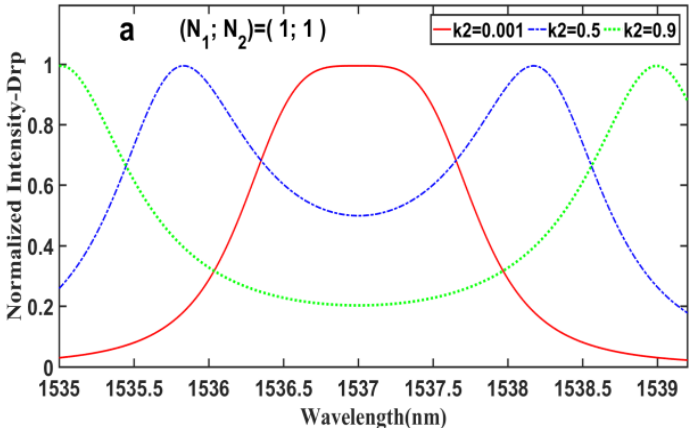
a
(N1; N2)=(1; 1)
k2=0.001
k2=0.5
k2=0.9
Normalized Intensity-Drp
Wavelength(nm)

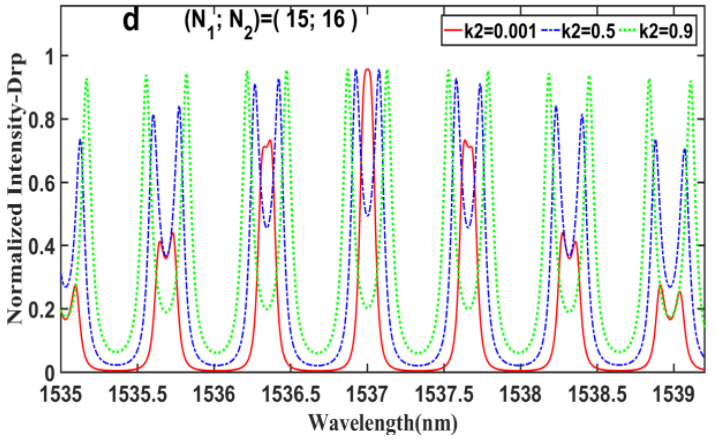
d
(N1; N2)=(15; 16)
k2=0.001
k2=0.5
k2=0.9
Normalized Intensity-Drp
Wavelength(nm)

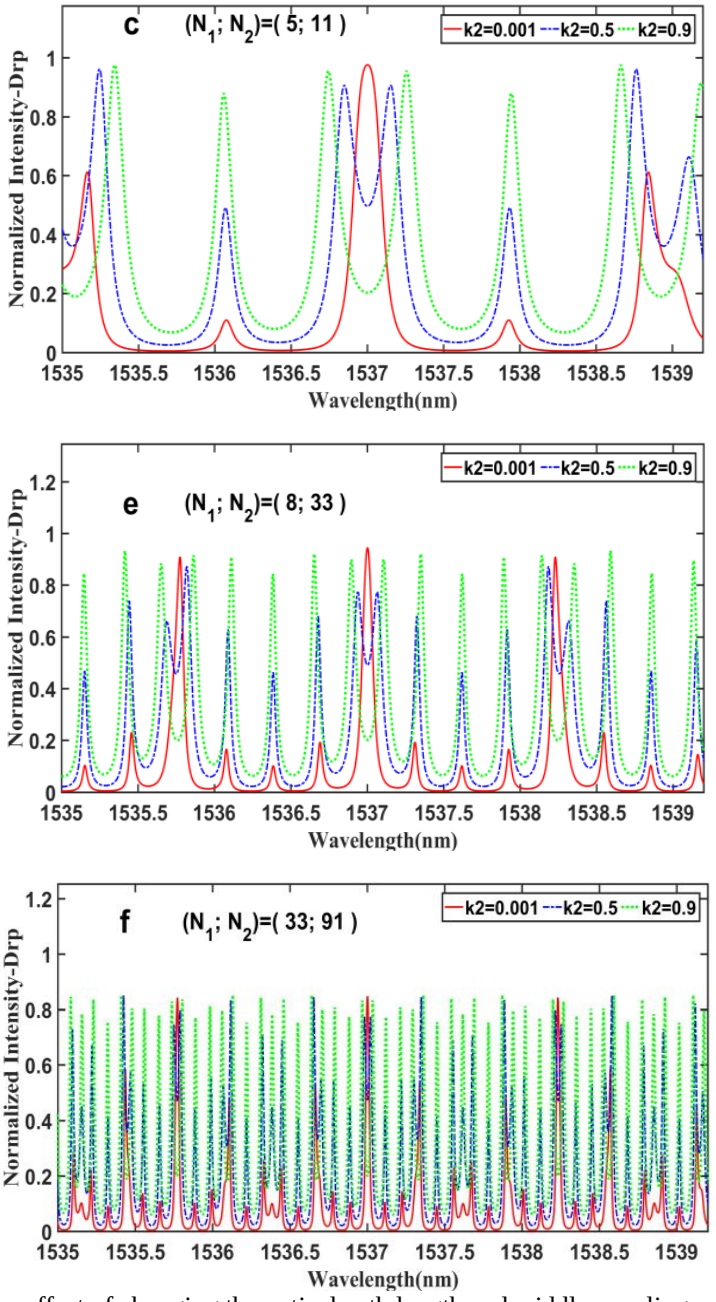

Fig. 4. The effect of changing the optical path length and middle coupling coefficient of DMR resonance peaks. *a)* (N1;N2)=(1;1). *b)* (N1;N2)=(2;5). *c)* (N1;N2)=(5;11). *d)* (N1;N2)=(15;16). *e)* (N1;N2)=(8;33) *f)* (N1;N2)=(33;91).

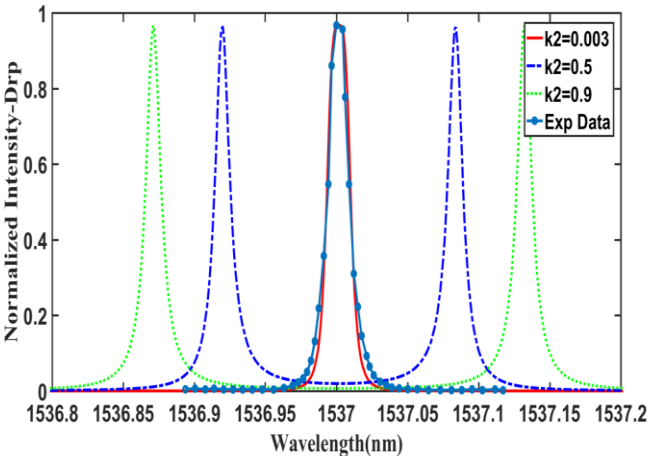

Fig. 5. Comparing the result from DMR system with experimental data.

In order to validate our results, a simulated result of the *DMR* system is compared with the experimental data reported in [18]. The DMR ring's radii are selected to be 150.8 μm and 160.8 μm from InGaAsP-InP waveguide material. The lateral couplings are set to be equal as *k1=k3=0.1*. Results are simulated for three sets of middle coupling coefficients of 0.003, 0.5and 0.9. The resonant peaks emerged in different locations based on the value of the middle coupler of the DMR. As shown in Figure5, the result for middle coupling coefficient of *k2=0.003*, resonant modes of 15 and 16, symmetric lateral coupling of 0.1 and waveguide loss of 6% is quite compatible with the measured experimental data from InGaAsP-InP double stage microring resonator[18]. It shows the conformity of our simulated results with the experimental data.

4. CONCLUSION

The behavior of light is studied through six different layouts of double microring resonators from InGaAsP-InP waveguide material. The effect of middle power coupling coefficient and resonant mode numbers on the output signals from DMR are studied. It is found that, increasing the power of middle coupling coefficient can generate dual resonant peaks. Additionally, it diminishes the free spectral range and causes the emergence of weak signals between main resonance peaks. Applying smaller values for middle coupler in the DMR brings about more suppression of resonances between main resonance peaks. Moreover, the width and height of the box like response are changed under the modification of the resonant mode numbers and middle coupling

coefficient. The simulated results are concordant with the experimental data. Obtained results can be used in optical communications.

REFERENCES

[1] M. Xiong, Y. Ding, H. Ou, C. Peucheret, and X. Zhang, *Comparison of wavelength conversion efficiency between silicon waveguide and microring resonator*, Frontiers of Optoelectronics, 9 (2016) 390-394.

[2] Z. Q. Hui, Y. Zhang, M. Yang, S. Wei, M. Zhang, and F. He, *Nonconcentric triple-microring resonator for label-free on-chip sensing with high figure-of-merit*, Journal of Nanophotonics, 11 (2017) 036014.

[3] S. Yoshida, S. Ishihara, Y. Nishijima, Y. Kokubun, and T. Arakawa, *Improved Sensitivity of Microring Resonator-Loaded Mach–Zehnder Interferometer Biosensor*, Sensors and Materials, 29 (2017) 1241-1246.

[4] M. Bahadoran, J. Ali, and P. P. Yupapin, *Ultrafast all-optical switching using signal flow graph for PANDA resonator*, Applied Optics, 52 (2013) 2866-2873.

[5] M. Bahadoran, J. Ali, and P. P. Yupapin, *Graphical approach for nonlinear optical switching by PANDA vernier filter*, IEEE Photonics Technology Letters, 25 (2013) 1470-1473.

[6] P. Yupapin, C. Teeka, M. A. Jalil, and J. Ali, *Nanoscale Nonlinear Panda Ring Resonator*: Science Pub Incorporated, 2012.

[7] G. P. Agrawal, *Nonlinear Fiber Optics*, Second Edition ed.: Academic Press, 1995.

[8] K. Oda, N. Takato, and H. Toba, *A wide-FSR waveguide double-ring resonator for optical FDM transmission systems*, Journal of Lightwave Technology, 9 (1991). 728-736.

[9] P. Yupapin, C. Teeka, and J. Ali, *Nanoscale nonlinear Panda ring resonator*: CRC Press, 2012.

[10] M. Bahadoran, A. F. A. Noorden, K. Chaudhary, F. S. Mohajer, M. S. Aziz, S. Hashim, J. Ali, and P. Yupapin, *Modeling and analysis of a microresonating biosensor for detection of Salmonella bacteria in human blood*, Sensors, 14 (2014) 12885-12899.

[11] M. Bahadoran, A. F. A. Noorden, F. S. Mohajer, M. H. Abd Mubin, K. Chaudhary, M. A. Jalil, J. Ali, and P. Yupapin, *Detection of Salmonella bacterium in drinking water using microring resonator*, Artificial cells, nanomedicine, and biotechnology, 44 (2016) 315-321.

[12] J. K. Poon, J. Scheuer, S. Mookherjea, G. T. Paloczi, Y. Huang, and A. Yariv, *Matrix analysis of microring coupled-resonator optical waveguides*, Optics Express, 12 (2004) 90-103.

[13] R. Orta, P. Savi, R. Tascone, and D. Trinchero, *Synthesis of multiple-ring-resonator filters for optical systems*, IEEE Photonics Technology Letters, 7 (1995) 1447-1449.

[14] M. Bahadoran, M. Aziz, A. Noorden, M. Jalil, J. Ali, and P. Yupapin, *Novel Approach to Determine the Young's Modulus in Silicon-On-Insulator Waveguide using Microring Resonator*, Digest Journal of Nanomaterials and Biostructures, 9 (2014) 1095-1104.

[15] J. Capmany and M. A. Muriel, *A new transfer matrix formalism for the analysis of fiber ring resonators: compound coupled structures for FDMA demultiplexing*, Journal of lightwave technology, 8 (1990) 1904-1919.

[16] M. Bahadoran, A. Afroozeh, J. Ali, and P. P. Yupapin, *Slow light generation using microring resonators for optical buffer application*, Optical Engineering, 51 (2012) 044601-8.

[17] M. Bahadoran, A. F. A. Noorden, K. Chaudhary, M. S. Aziz, J. Ali, and P. Yupapin, *Nano force sensing using symmetric double stage micro resonator*, Measurement, 58 (2014) 215-220.

[18] S. J. Choi, Z. Peng, Q. Yang, S. J. Choi, and P. D. Dapkus, *Tunable narrow linewidth all-buried heterostructure ring resonator filters using Vernier effects*, IEEE Photonics Technology Letters, 17 (2005) 106-108.